Modal Dynamics for Space-Division Multiplexing in Multi-Mode Fibers

Rekha Yadav, Fabio A. Barbosa, *Member, IEEE, Member, Optica,* and Filipe M. Ferreira, Senior *Member, IEEE, Member, Optica*

***Abstract*—We introduce a new drift model for slow environmental perturbation affecting modal coupling in optical multi-mode fibers. This model preserves the mode coupling strength asymmetries characteristic to mode pairs of different mode groups while decorrelating the fiber transmission matrix. Existing drift models were derived for the strong coupling regime, in which case the coupling matrix elements are identically distributed, and not suitable for the weak to intermediate coupling regime as shown here. The models' impact on the inherent crosstalk characteristic of a fiber were evaluated for all linear coupling regimes and for fibers with up to 42 spatial and polarization modes. Moreover, transmission performance of 32 GBd 16-QAM (per polarization mode) over the dynamic channel is studied considering singular value decomposition (SVD) pre-coding for the multiple-input multiple-output multi-mode fiber channel. The impact of slow drift on channel equalization performance is evaluated in terms of residual crosstalk. A large discrepancy is observed for fiber channels in the weak and intermediate coupling regimes, while converging in the strong coupling regime. Furthermore, we show that 2 × 1 multiple-input single-output equalizers can be sufficient to compensate for the residual crosstalk in the weak to intermediate linear coupling regime and achieve optimal performance.**

***Index Terms*—Space-division multiplexing, multi-mode fiber, linear mode coupling, dynamic channel.**

I. Introduction

Space-division multiplexing is one of the advanced technologies being considered to fulfil the increased demand of information transfer where data co-propagates in the parallel spatial pathways making the use of shared resources [1-5] and which includes parallel cabled single-mode fibers, multi-core fibers (MCFs), multi-mode fibers (MMFs) as well as few-mode multi-core fibers. MMFs allow for tenths-to-hundreds of spatial pathways while keeping to a standard cladding diameter of 125 μm – allowing for higher production yield and smaller mechanical failure rates [6-8]. While coupled-core MCFs allow for only ~19 spatial pathways [2] when keeping to a standard cladding diameter.

Despite larger bandwidth density, multi-mode fibers have significant modal walk-off (~10-100 ps/km) and linear mode coupling (LMC) due to fiber imperfections [9]. The combination of these effects increase the equalization complexity requirements at the receiver end [10]. Nevertheless, these impairments can be overcome in systems using coherent detection with digital signal processing (DSP) including multiple input multiple output (MIMO) equalizers. Several works model the LMC as small deviation in the core-cladding boundary that arises from the perturbations introduced in the fabrication process [9-11]. In these models, the fiber channel is divided into multiple sections of small step length with LMC, and dispersion being applied separately, following the split-step Fourier method.

Environmental processes such as temperature fluctuations affect the overall fiber transfer function [12-16]. And so, the study of these effects in transmission systems is required to understand the effect of slow and fast time varying perturbations in field deployment where the channel is not stable [17-25]. These perturbations directly impact the need for channel re-estimation implying increase in the DSP latency and power consumption or decrease in the spectral efficiency. Recently, the effect of environmental perturbations on multi-mode SDM transmission systems was studied for channels in the strong linear coupling regime [26]. Whereas, multi-mode fibers, and in particular few-mode fibers operate in the weak to intermediate regime (for metro-haul distances) [27-29].

In our previous work, we have proposed a stochastic model taking account of channel drift keeping the modal coupling strength asymmetries between mode pairs (e.g., intra-mode group vs inter-mode group) [30]. Here, we extend our previous work by expanding the description and analysis of the fiber model to include the polarization treatment and analyze the required perturbation strength for different numbers of sections and modes. Critically, the analysis here considers data transmission (as opposed to single-frequency operation) for a singular value decomposition (SVD) system over the MIMO fiber channel. With an SVD-MIMO system, channel state information (CSI) is needed at the transmitter, and so latency in the CSI transmission means that channel diagonalization will be based on an outdated channel estimate. The impact of the latter is evaluated by the new drift model proposed.

The manuscript is organized as follows. Section II introduces the modelling of the multi-mode fiber channel, neglecting the dynamic effects. Section III describes the procedure to model slowly time varying changes in the multi-

Submitted to IEEE/Optica Journal of Lightwave Technology on September 14th, this work was supported by the UKRI Future Leaders Fellowship [MR/T041218/1]; Engineering and Physical Sciences Research Council (EPSRC) Doctoral Studentship Grant reference [EP/R513143/1] and [EP/W524335/1]. (Corresponding author: Rekha Yadav).

The authors are with the Optical Networks Group, Department of Electronic and Electrical Engineering, University College London (UCL), London WC1E7JE, UK. (e-mail: rekha.yadav.22@ucl.ac.uk, fabio.barbosa@ucl.ac.uk, f.ferreira@ucl.ac.uk). Color versions of one or more figures in this article are available at https://doi.org/xxxx. Digital Object Identifier xxxx.

mode fiber channel. This section also discusses the effect of perturbation strength in the lumped and distributed manner, deriving a relationship between them. Section IV discusses the implications on crosstalk for single-frequency transmission over time-varying fiber channel. Section V presents the simulation results for the transmission of polarization mode multiplexed 16-QAM signals over a dynamic channel, quantifying the performance in terms of signal-to-noise ratio. And we draw conclusions in Section VI. Note that throughout the manuscript, mode counting refers to spatial modes: this is, a fiber which supports LP_{01} and LP_{11} will normally be said to support two LP modes, three spatial modes and six polarization modes.

II. Modelling the Multi-mode Fiber Channel

For the unperturbed dielectric waveguide, the propagating field can be expressed in the frequency do*m*ain as a linear combination of the ideal modes $\tilde{\boldsymbol{E}}(x,y,z,\omega) = \sum \tilde{A}_m(z,\omega)\tilde{\boldsymbol{E}}_m(x,y)$ where m is the polarization mode index, $\tilde{A}_m(z,\omega)$ is the Fourier transform of the slowly varying mode field envelope $A_m(z,t)$ and $\tilde{\boldsymbol{E}}_m(x,y)$ is the Fourier transform of the ideal electric field distribution ($\boldsymbol{E_m}(x,y)$) – assuming the waveguide is constant along z. In the presence of a time-invariant dielectric perturbation $\Delta\varepsilon(x,y,z)$, the coupling between the ideal modes is described by the following coupled-mode equations [11, 31-34], expressed here in the matrix form:

$$\hat{\partial}\tilde{\mathbf{A}}(z,\omega) = -\mathrm{j}[\boldsymbol{\beta}(z,\omega) + \mathbf{K}(z) + \mathbf{R}(z)]\,\tilde{\mathbf{A}}(z,\omega) \qquad (1)$$

where $\tilde{\mathbf{A}}(z,\omega)$ is a column matrix whose m-th element is $\tilde{A}_m(z,\omega)$; $\boldsymbol{\beta}$ is a diagonal matrix whose m-th element is the frequency dependent propagation constant (β_m) of mode m at a frequency ω. $\mathbf{K}$ is the mode coupling matrix where the (m,n) element is given by the area integral of the inner product of the electrical fields of mode m and mode n, over the area where the permittivity perturbation $\Delta\varepsilon(x,y,z) \neq 0$ as shown below

$$K_{m,n}(z) = \omega\varepsilon_0/4 \iint \Delta\varepsilon(x,y,z)\, \boldsymbol{E_m}^*(x,y)\cdot\boldsymbol{E_n}(x,y)dx\,dy \qquad (2)$$

and, ε_0 represents the permittivity in free space. And, $\mathbf{R}$ is a block diagonal matrix composed of 2×2 submatrices, where m submatrix is defined by $\boldsymbol{\alpha_m}(z)\cdot\boldsymbol{\sigma}(z)$ [12, 13] with $\boldsymbol{\alpha_m} = \theta_m\,\hat{a}_m$, θ_m is angular displacement between [0,π) over a 3-dimensional vector $\hat{a}_m$ in an unit sphere, and finally $\boldsymbol{\sigma} = (\boldsymbol{\sigma_1}, \boldsymbol{\sigma_2}, \boldsymbol{\sigma_3})$ is a tensor of the Pauli spin matrices with $\boldsymbol{\sigma_1} = [1\ \ 0;\ 0\ \ -1]$, $\boldsymbol{\sigma_2} = [0\ \ 1;\ 1\ \ 0]$ and $\boldsymbol{\sigma_3} = [0\ \ -j;\ j\ \ 0]$.

An approximate solution of (1) can be obtained by assuming that modal dispersion and linear mode coupling act independently in the fiber for a sufficiently small step [11]. This is, that over dz, the walk-off induced by chromatic or modal dispersion is much smaller than the pulse width. Finally, for a given fiber section i of length dz, by neglecting dispersive effects and assuming $\boldsymbol{\beta}$, $\mathbf{K}$ and $\mathbf{R}$ constant over dz, the fiber transfer matrix is given by the exponential matrix [32] as

$$\tilde{\mathbf{M}}_i(\omega) = \exp\left(-\mathrm{j}[\boldsymbol{\beta_0} + \mathbf{K} + \mathbf{R}]dz\right) \qquad (3)$$

where $\boldsymbol{\beta_l}$ is a diagonal matrix whose m-th element is the l-th order coefficient of a Taylor series expansion of mode m propagation constant $\beta_m(\omega)$ centered at the carrier frequency ω_0. In this manuscript, β_m and $K_{m,n}$ are obtained from the refractive index profiles optimized for low modal group delay, for a graded index fiber with a cladding trench as described in [5] with core radius of 22.90 µm, core to trench distance as 1.75 µm, trench width as 5.25 µm, trench depth as -0.0021 µm, α core graded-index exponent as 1.96 and core-cladding refractive index relative difference as 0.0045. In our previous work, we have considered for $\mathbf{R}$, that $\boldsymbol{\alpha_m}\cdot\boldsymbol{\sigma}$ is the same across all modes, for the given i-th fiber section. It has been reported that when polarized light is launched in a multi-mode fiber, each spatial mode experiences different polarization evolution [34-36]. Therefore, we consider here different $\boldsymbol{\alpha_m}\cdot\boldsymbol{\sigma}$ for every mode, at each i-th fiber section. β_m are kept constant over all fiber sections while $K_{m,n}$ changes given a random radial and azimuth offset in each section [11]. Finally, the end-to-end fiber transfer matrix is obtained as the product of each section's transfer matrix given by $\tilde{\mathbf{M}}_i(\omega)$ in (3), this is $\mathbf{H} = \tilde{\mathbf{M}}_N(\omega)\cdot\tilde{\mathbf{M}}_{N-1}(\omega)\cdot\tilde{\mathbf{M}}_{N-2}(\omega)\ldots\cdot\tilde{\mathbf{M}}_1(\omega)$, where N represents the total fiber sections [37].

In MMFs, the mode coupling strength can be quantified as the ratio between the average power in all the other modes and that remaining in the launching mode(s), after a certain distance. However, mode coupling strength should also take into consideration the receiver architecture. Take the following scenario: (A) For mode group division multiplexing with separate MIMO equalizers for each mode group and with MIMO order matching each mode group cardinality [24, 38, 39], intra-mode group coupling can be fully compensated and so only interference from outside the group limits transmission performance. In this case, one can define crosstalk as the ratio between the average power of all the modes in the other mode groups and that remaining in the targeted mode group.

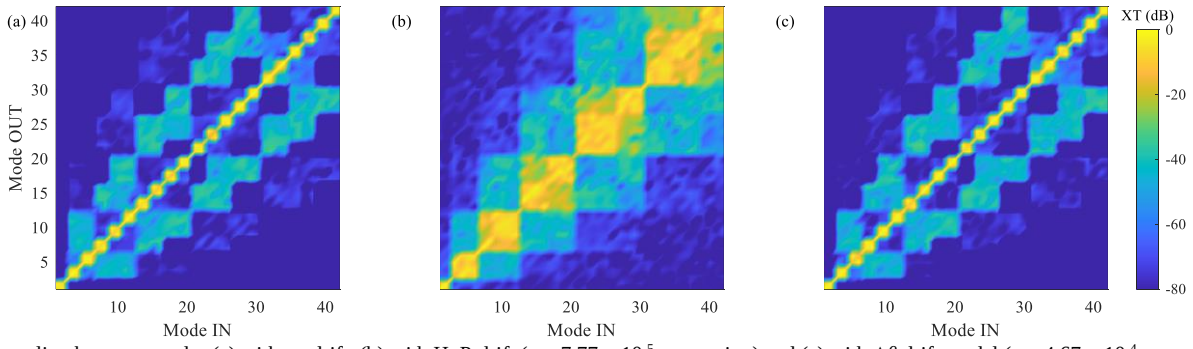

Fig. 1. Power coupling between modes (a) without drift, (b) with HoP-drift ($\kappa = 7.77 \times 10^{-5}$ per section) and (c) with $\Delta\beta$-drift model ($\kappa = 4.67 \times 10^{-4}$ per section) for a fiber with 42 polarization and spatial, 10 km long, crosstalk strength as -40 dB/km, dz = 1 m and $\delta t/T_{env} = 1$.

(B) Another potential scenario considers MIMO equalization on groups of degenerate modes only, e.g.: (LP_{21ax}, LP_{21ay}, LP_{21bx}, LP_{21by}) or just (LP_{21ax}, LP_{21ay}). In this case, one can define crosstalk as the ratio between the average power of all the other modes that are non-degenerate and that of the modes that are degenerate with given target mode(s). So, the mode coupling strength definition for all the cases in multi-mode fibers is:

$$XT_m = \sum_{v \neq m} P_v \,/\, P_m \tag{4}$$

where P_v is the power of mode set v, after a given fiber segment under test, when only the mode set m is (partially or fully) launched – where mode set m is specific to the scenario under consideration, see scenario (A) and (B) above. Typical XT values of experimentally characterized few-mode fibers range from -40 dB/km to -30 dB/km for graded index fiber profiles [11, 40, 41], while for coupled-core fibers these can be substantially larger -18dB/km to -7dB/100m [42, 43]. Here, we consider mode set of interest as the polarization-degenerate modes together (e.g., LP_{21ax}, LP_{21ay}) for each mode m. Fig. 1 (a) shows a 21-mode fiber transmission matrix for 10 km length with XT strength as - 40 dB/km where each section length is considered as 1 m. It is observed that the coupling matrix in Fig. 1 (a) is more sparse and structured from the one shown in [28](supplementary material), for the experimental characterization of fiber. But characterization of fibers is challenging as one would require perfect mode multiplexer and demultiplexer such as one consisting of an aberration free system and a set of phase masks with infinite resolution. Instead in many cases, one uses an LCoS spatial light modulator (SLM) with as many as 8-bit / 10-bit phase resolution and a limited filling factor, among other shortcomings – which is the case in [28]. Here, we have assumed a perfect mode launching condition. Also, the authors in [28] have considered Laguerre Gaussian mode basis which are approximate solutions assuming weak guidance with the infinite core radius, whereas we have considered transmission of linearly polarized modes with a finite radius graded core including a cladding trench as described in [5].

III. Modelling of Environmental Perturbation

A. Homogenous perturbation drift model

The slow drift perturbation model proposed in [26] considers a channel in the strong coupling regime with the i-th section of the drifted channel described as:

$$\tilde{\mathbf{M}}_i(\omega,\delta t) = \text{expm}\left(\mathbf{M_{sh}} + \mathbf{M_{pert}}\,(\kappa\,\delta t \,/\, T_{env})^{1/2}\right) \tag{5}$$

where $\mathbf{M_{sh}}$ and $\mathbf{M_{pert}}$ are random skew-Hermitian matrices for fiber channel and drift perturbation, respectively. In [26], $\mathbf{M_{sh}}$ and $\mathbf{M_{pert}}$ are generated in the same manner: the real part and imaginary part of the elements in these matrices follow independent Gaussian random variables of zero mean and variance one. However, instead of $\mathbf{M_{sh}}$, here we have -j[$\boldsymbol{\beta}_0$ + $\mathbf{K}$ + $\mathbf{R}$]dz following our fiber channel model. And, κ is the perturbation variance required for channel matrix correlation to become smaller than e^{-2} when the change in time δt equals the characteristic time (T_{env}). We refer to this model as homogenous perturbation drift model (HoP-drift). The HoP model has been proven reliable for fibers in the strong coupling regime and with all guided modes being quasi-degenerate [25]. However, in the weak-to-intermediate coupling regime the variance of the elements of the coupling matrix is not homogeneous as crosstalk is strongest for modes in the same group, followed by coupling between modes of adjacent groups. Thus, applying a homogeneous perturbation artificially introduces coupling between sets of modes whose coupling strength should have remain negligible otherwise. We investigate this model for the physics-informed channel transmission matrix as discussed in section II. Fig. 1 (b) shows the 21-mode fiber transmission matrix from Fig. 1(a) after applying HoP-drift while considering $\delta t/T_{env} = 1$ (to achieve decorrelation, $\kappa = 7.77 \times 10^{-5}$ per section). Comparing Fig. 1 (b) to Fig. 1 (a), the enhanced crosstalk is evident overall and for intra-mode groups and neighboring mode groups due to the homogeneous perturbation added in the HoP-drift.

B. Proposed drift model: propagation constant based

Here, we propose an alternative slow-drift model to accommodate multi-mode optical fibers operating in all coupling regimes. The drift perturbation is applied only to β_m keeping $K_{m,n}$ unchanged by the effect of time-varying perturbation. In this way, we are accounting for slow drift perturbations such as temperature drift that are known to directly lead to changes on fibers refractive index and so on modes propagation constant $\beta_m \approx n \cdot 2\pi/\lambda$. While $K_{m,n}$ changes are neglected here since these are mostly determined by *relative* refractive index, see (2). The model proposed here, referred to as $\Delta\beta$-drift model, can be described as:

$$\tilde{\mathbf{M}}_i(\omega,\delta t) = \text{expm}\Big(\text{-j}[(\boldsymbol{\beta}_0 + \mathbf{K} + \mathbf{R})\,dz + \Delta\boldsymbol{\beta}\,(\kappa\,\delta t \,/\, T_{env})^{1/2}\,]\Big) \tag{6}$$

where $\Delta\boldsymbol{\beta}$ is a diagonal matrix containing the perturbation in the propagation constants, for the i-th section, whose elements are independent real Gaussian random variables of unit variance, and κ is the perturbation strength required to achieve correlation of e^{-2} between the non-drifted and drifted channel for $\delta t = T_{env}$, as defined in the previous section. Typical values for the characteristic timescale of channel drift in multi-mode fibers are still a subject of research with a wide range of values reported, from long-term stability of principal modes in [28] to shorter timescales associated with the digital holography characterization acquisition time ($\sim 0.1 - 100$s) [44]. Fig. 1 (c) shows the fiber transmission matrix after 10 km with XT as - 40 dB/km when drift is introduced using $\Delta\beta$-drift model, for $\delta t/T_{env} = 1$ (to achieve decorrelation, $\kappa = 4.67 \times 10^{-4}$ per section). Comparing Fig. 1 (c) to Fig. 1 (a), it can be observed that the XT asymmetries between mode groups remain unchanged with time despite having a decorrelated channel matrix.

C. Correlation vs perturbation strength: single fiber section

First, we analyzed the perturbation strength required in each model to decorrelate the end-to-end fiber propagation matrix for a single fiber section. The scalar correlation metric $C(\delta t)$ is

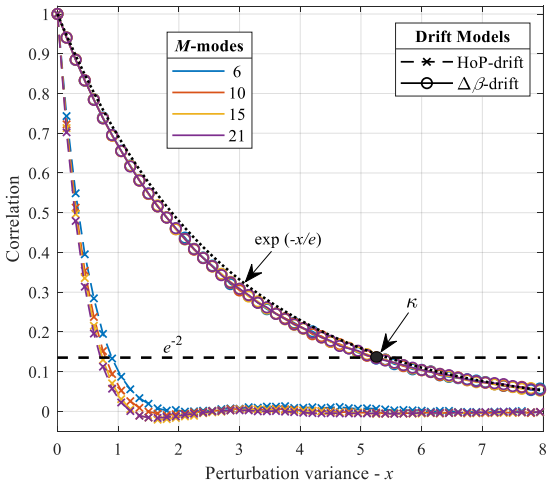

Fig. 2. Transmission matrix correlation as a function of the perturbation strength for a single section fiber with (6,10,15,21) spatial modes and XT = -40 dB/km, considering $dz = L$ = 1 m – for both drift models. Results averaged over for 10,000 fiber realizations.

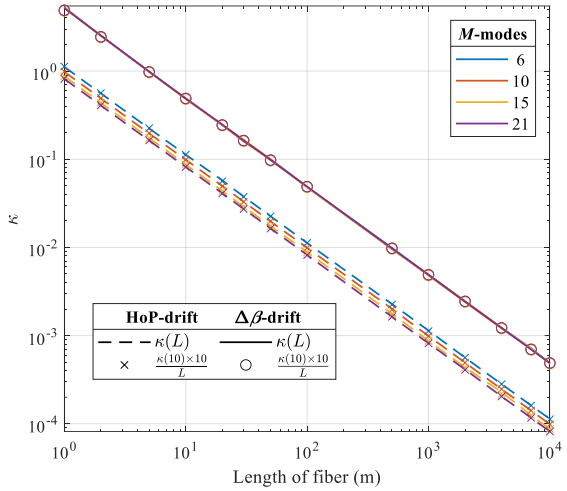

Fig. 3. Variation of κ with fiber length for both drift models considering fibers with (6,10,15,21) spatial modes, dz = 1 m, and XT = -40 dB/km. Results averaged over 1000 different fiber runs.

defined as in [26], $C(\delta t) = \text{trace}(\mathbf{H}(t)[\mathbf{H}(t+\delta t)]^{H}) / (2M)$, where $\mathbf{H}$ is the end-to-end transfer matrix as described in Section II accounting for the drift following $\tilde{\mathbf{M}}_i(\omega,\delta t)$ given by (5) or (6), for $2M$ polarization modes (e.g. For the modes in a fiber with LP_{01}, LP_{11a}, and LP_{11b}, $2M$ corresponds to 6 polarization modes) supported in a given fiber. Importantly, here we define the perturbation variance required κ to achieve channel matrix decorrelation as $C(T_{env}) \approx e^{-2}$. This is similar to polarization mode dispersion theory [45] where the correlation length is defined to be the length at which the average power in the orthogonal mode is within e^{-2} of the power in the starting mode.

Fig. 2 shows the channel correlation, as a function of the applied perturbation strength, between the non-drifted channel at $\delta t = 0$ and the channel drifted with the varying perturbation strength – for a single fiber section of length 1 m with XT strength as -40 dB/km and different number of spatial mode fibers, considering $\delta t/T_{env} = 1$. For the $\Delta\beta$-drift model, we observe that the correlation decays exponentially with the perturbation strength and that such decay is not impacted by the number of modes or crosstalk (shown by further results over all coupling regimes). The exponential decay follows that of correlated log-normal random variables, but it deviates given $\boldsymbol{\beta}$ and $\mathbf{K}$ characteristic to a given fiber profile type. In Fig. 2, and for the group of fibers considered, correlation approximately follows $\exp(-x/e)$ where x is the applied perturbation variance to the fiber. For the HoP-model, the correlation dependency on the perturbation strength follows that in [26], except that here by including $\boldsymbol{\beta}$ (so, diagonal terms are now much larger than the off-diagonal) the dependency on the number of modes is much reduced. Moreover, in Fig. 2, we also observe that the perturbation strength required for decorrelation is larger for the $\Delta\beta$-drift model than that for the HoP-model. This can be understood by noting that in the former case the perturbation takes the form of a diagonal matrix while in the latter case the perturbation takes the form of a dense matrix, see Section II.

D. *Correlation vs perturbation strength: multi fiber section*

For the multi-section dynamic fiber model discussed here, independent perturbation sources (Gaussian random variables) of the same perturbation variance (κ) are assumed acting on each fiber section. Correlation between the non-drifted channel (t = 0) and drifting channel is calculated for a given length of the fiber from the end-to-end fiber transfer matrix as described in Section III-C. κ is the perturbation variance required per section to decorrelate the full-length fiber channel. Therefore, the κ value per section decreases as number of fiber sections increases (L/dz), which is the case when increasing the fiber length (L) or reducing the section length (dz). This is confirmed in Fig. 3 that shows the variation of κ with fiber length for a set of fibers with (6, 10, 15, 21) spatial modes and considering section length as 1 m. We observe that κ per section required for decorrelation of a given fiber length in a multi-section model follows κ of single section fiber length by dz/L (i.e., 1/#sections) – doubling the number of sections corresponds to halving κ. This implies that the product of random matrices (5) or (6) has its central limit as the exponent of a Gaussian unitary ensemble. That would be the case when (5) and (6) can be approximated by $\mathbf{I} + \delta\mathbf{X}$ with a very small δ [37], such that: $\log \mathbf{AB} \approx \log \mathbf{A} + \log \mathbf{B}$, where $\mathbf{A}$ and $\mathbf{B}$ are given by (5) or (6). We noticed that the required κ only deviates from a dz/L dependency for $dz \approx L$, it deviates by over 5%. For this reason, we take the required κ for 10 m as the reference, and in the following, the required κ for an arbitrary length L is obtained as: κ (10 m) × 10 m / L.

IV. Effect of Slow Perturbations on Single Frequency Channel

In this section, we discuss the effect of the proposed drift model on the multi-mode fiber channel for single-section and multi-section fiber cases as well as for an SVD system case; always considering single-frequency operation.

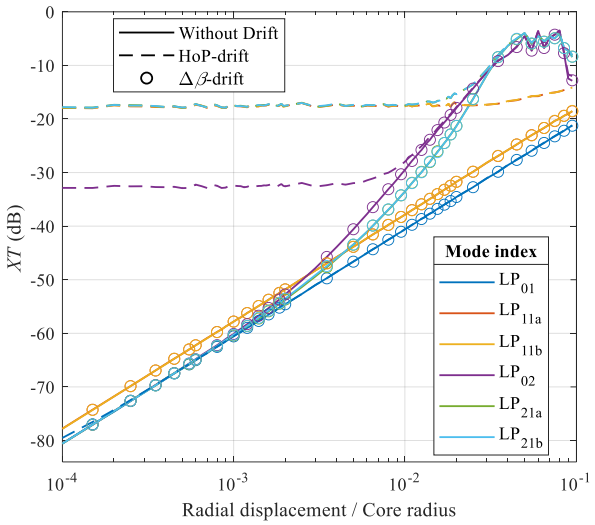

Fig. 4. *XT* for mode *m* as a function of radial displacement (and averaged over the angular displacement) for a fiber with 6 spatial modes and $\delta t/T_{env} = 10^{-2}$. Results averaged over 100 different drift realizations.

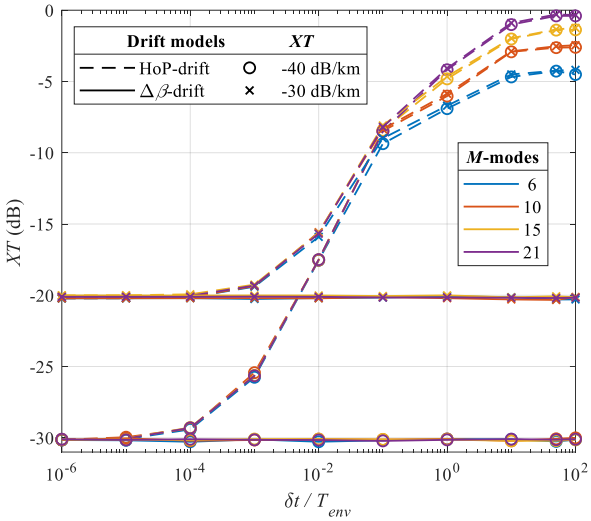

Fig. 5 *XT* at the fiber output averaged over all modes as a function of $\delta t/T_{env}$ for a 10 km fiber with (6, 10, 15, 21) spatial modes considering a crosstalk strength of -40 dB/km and -30 dB/km for both drift models. Results averaged over 100 different fiber realizations.

A. *Single- and multi-section analysis*

First, by considering a single step of 1 m length, we analyze the crosstalk for a 6 spatial mode fiber considering $\delta t/T_{env} = 10^{-2}$. Fig. 4 shows the evaluated *XT* for each mode set *m*, composed by both polarizations of a given spatial mode, as a function of the normalized radial displacement, where each point has been averaged over the range of azimuthal displacement and polarization rotation values, following [11] for a random realization of drift each time. We observe that with $\Delta\beta$-drift model, *XT* strength remains the same as for the case without drift for all the radial displacement values. Whereas for small values of radial displacement ($\lesssim 10^{-2}$), it can be observed that with the HoP-drift model degenerate modes have highest crosstalk, followed by the modes in higher mode groups. These modes are characterized by small propagation constant differences and small $K_{m,n}$, and therefore when applying homogeneous perturbation these are most affected. However, from the experimental work in [28], one expects the overall mode coupling strength should remain identical over time – note that the principal modes associated with a given fiber coupling matrix remain "quite stable" over long periods of time as long as 6 months apart. But this would not be the case with the drift-induced crosstalk increase observed for the HoP-model in Fig. 4, and this conveys that HoP-drift model is not suitable for the weak to intermediate coupling regimes.

Further, we investigate the effect of drift with time evolution for a multi-section fiber case with drift being applied to each section for both the drift models as discussed in Sections II and III. Fig. 5 shows *XT* as a function of $\delta t/T_{env}$ for a 10 km long fiber with a crosstalk strength of -40 dB/km and -30 dB/km – results averaged over 100 different fiber realizations. We can observe from the Fig. 5 that *XT* remains at the crosstalk strength level inherent to the fiber for the $\Delta\beta$-drift model and this coincides with the experimental work shown in [28] – as discussed in the previous paragraph, whereas *XT* with the HoP-drift model increases quickly beyond this level for $\delta t/T_{env}$ values larger than 10^{-5} and 10^{-4} for the fibers considered respectively, with (6, 10, 15, 21) spatial modes. We also observe in Fig. 5 that HoP-drift model produces equivalent results to those of $\Delta\beta$-drift even in weak-to-intermediate coupling for smaller $\delta t/T_{env}$ ($\lesssim 10^{-4}$), limiting the range of slow perturbations that can be accounted.

B. *Transmission system analysis*

In transmission systems, channel equalization is necessary to unravel the coupling introduced by the channel and recover the

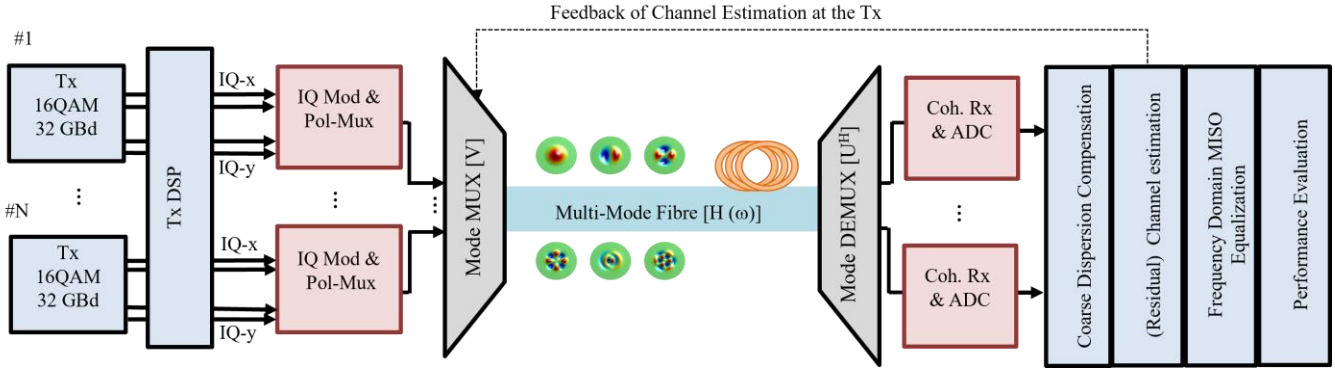

Fig. 6 Simulation setup considered for signal transmission over multi-mode fibers and DSP steps involved in the processing of data. Tx and Rx represents transmitter and receiver respectively.

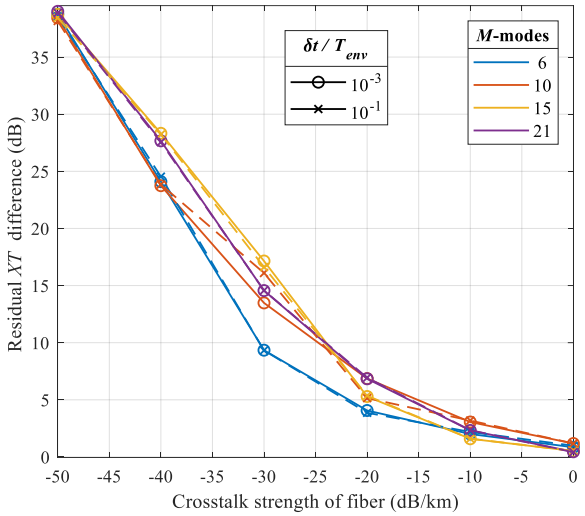

Fig. 7 *XT* residual averaged over all modes as a function of fiber crosstalk strength considering $\delta t/T_{env} = 10^{-3}$ and 10^{-1} respectively. Results averaged over 500 fiber realizations.

spatial tributaries launched. An optimal solution to interference-limited MIMO systems is the singular value decomposition (SVD) approach – used here for simplicity and without lack of generality. In the SVD approach, one diagonalizes a given channel matrix into two unitary matrices (**U** and **V**), and a diagonal matrix (**Λ**). The unitary matrices **V** and $\mathbf{U}^{H}$ can be applied at the transmitter and the receiver, respectively, to diagonalize the channel response. Further, we calculate the unitary matrices $\mathbf{U}(\delta t=0)$ and $\mathbf{V}(\delta t=0)$ in SVD for the channel without drift perturbation, which is $\mathbf{H} = \mathbf{U}\boldsymbol{\Lambda}\mathbf{V}^{\mathbf{H}}$, and then apply these to the drifted channel after a certain time (δt). This time delay accounts for the fact that in the SVD approach channel the state of information must be exchanged between the transmitter and the receiver as illustrated in Fig. 6. With this approach, the residual channel at the input of the receiver becomes,

$$\boldsymbol{H}_{res}(\omega,\delta t) = \boldsymbol{\Lambda}^{-1}(\omega,0)\mathbf{V}(\omega,0)\boldsymbol{H}_{drifted}(\omega,\delta t)\mathbf{U}^{H}(\omega,0) \qquad (7)$$

where $(.)^{H}$ is the Hermitian operator. From $\boldsymbol{H}_{res}$ in (7) one can evaluate the residual *XT* induced by channel drift.

Fig. 7 shows the difference in *XT* residual between the HoP-drift model and the $\Delta\beta$-drift model varying the crosstalk strength of the fiber, considering the $\delta t/T_{env} = 10^{-3}$ and 10^{-1} for a 10 km fiber. We observe that the difference in residual *XT* is particularly high (as much as 25 dB to 5 dB) in the weak to intermediate range (-40dB/km to -20dB/km) and decreases with the increase in the crosstalk strength of the fiber. As the crosstalk strength increases, the modal coupling between the modes of all the groups tends to become uniform and applying a uniform drift perturbation (HoP model) would behave similar to applying perturbation in the propagation constants ($\Delta\beta$-drift model). This confirms that the performance of both the drift models coincide in the strong coupling regime, whereas there is a large difference in the weak to intermediate coupling regime. Finally, in Fig. 7, the residual *XT* level for $\Delta\beta$-drift model is not following a specific trend with the number of modes, this is not unexpected since the fibers used here were optimized for minimum group delay only [5], no consideration on linear mode coupling is included during fiber profile optimization.

V. Effect of Slow Perturbations on Modulated Signal Transmission

In this section, we quantify the effect of slow perturbations when a 16-QAM signal is transmitted over a fiber channel of length 10 km with a step length of 1 m. Simulation setup is shown in Fig. 6 where an initial transmission of 32 GBd 16-QAM is performed, considering an ideal transmitter, the signal is launched in the fiber experiencing the modal dispersion, modal coupling and polarization rotation at each step. The amplified spontaneous emission (ASE) noise is added to the signal just before coherent detection such that OSNR in the reference bandwidth of 12.5 GHz is set to 35 dB for all detected modes. The received signal is then processed for the dispersion compensation, and the (residual) channel matrix is acquired – since in this manuscript the focus is on the drift-induced performance penalty, the calculated channel is used at this point. This channel matrix is then used to diagonalize the end-to-end channel using SVD as discussed in Section IV. In this way, the generated 32 GBd 16-QAM signal is pre-processed by multiplying it with the unitary matrix (**V**) in frequency domain, before transmission over the fiber. But on this turn around, the fiber channel has been perturbed in the manner discussed in Sections II and III. All the modes experience the chromatic and modal dispersion as presented in [5]. After fiber transmission, the received signal is then equalized using unitary matrix ($\mathbf{U}^{H}$) of SVD for compensating the fiber channel. The residual received signal is then processed using frequency domain equalizer for chromatic dispersion compensation taking account the mean value of chromatic dispersion coefficient for all the modes. And, to compensate for the residual modal coupling after SVD we use MISO equalization. A frequency domain based MISO equalizer utilizing an overlap-save method with a 1024-point fast Fourier transform and an overlap of 2 samples [46]. The input mode set to the MISO equalizer for a particular output spatial polarization tributary is chosen by the maximum cross-correlation (this is, the largest interferers). Finally, the *signal-to-noise ratio* (*SNR*) is calculated from the received constellation with respect to the transmitted signal given as $SNR = E[|X|^2] / E[|Y - X|^2]$ where *X* and *Y* are the transmitted and received symbols after equalization, respectively, and E[.] denotes the expectation operator.

Fig. 8 shows the *SNR* of the received signal (after SVD and MISO equalization), averaged over the modes, as a function of the number of inputs to the MISO equalizer with both the drift models, considering $\delta t/T_{env} = 10^{-1}$ for 32 GBd, 16-QAM transmission per spatial polarization for 10 km long fibers supporting (6, 10, 15, 21) spatial modes and *XT* as -40 dB/km at an *OSNR* of 35 dB. We can observe that for the $\Delta\beta$-drift model *SNR* approaches the maximum possible value (given the *OSNR*) with just 2 × 1 MISO – this is when the drift leads residual crosstalk among two polarization modes mostly. While for the HoP-drift model, the required equalizer size to approach maximum *SNR* is 4 or more given the model's impact on four-fold degenerate modes (e.g., LP_{21}), see Fig. 4. And so,

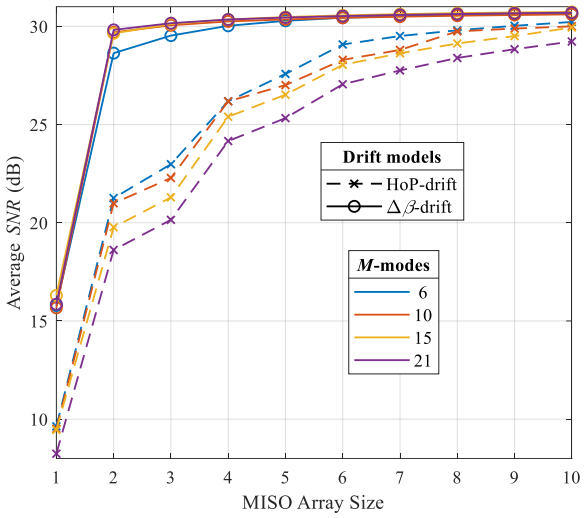

Fig. 8. *SNR* as a function of MISO array size considering *XT* as -40 dB/km, L = 10 km and $\delta t/T_{env} = 10^{-1}$. *SNR* averaged over all modes and 100 different fiber realizations.

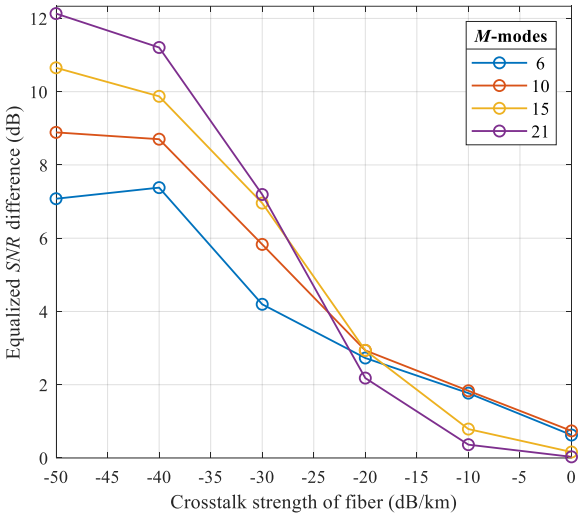

Fig. 9 Difference in equalized *SNR* between drift models as a function of fiber crosstalk strength with 2 × 1 MISO and $\delta t/T_{env} = 10^{-1}$. Results averaged over all modes for 100 different fiber realizations.

for 2 × 1 MISO, the *SNR* difference between the two models for the system described in Fig. 8 can be as larger as 12 dB for $\delta t/T_{env} = 10^{-1}$, as in for 21 spatial modes. For smaller $\delta t/T_{env}$ values, the *SNR* difference becomes smaller, but it remains larger than 3dB at $\delta t/T_{env} = 10^{-3}$. This difference illustrates the importance of the drift modelling assumptions for system performance estimation. The $\Delta\beta$-drift model indicates that a SVD-like approach may remain effective in suppressing the modal mixture of non-degenerate modes for large $\delta t/T_{env}$ (e.g., $\delta t/T_{env} \approx 0.1$). Furthermore, we believe that low order MISO approach would still be effective for other fibers, for example, Figure S5(b) in [28] shows that by applying a conjugated transpose manipulation only a few off-diagonal interferers remained visible for a 72-mode fiber. This is expectable even for longer lengths (~10km) since the modes of graded-index fibers can be organized into mode groups that are effectively independent, even over kilometers of fiber [39, 47, 48].

Further, we analyze the effect of fiber mode crosstalk on the system performance but with fixed MISO cardinality at 2 × 1, keeping fiber length at 10 km and $\delta t/T_{env} = 10^{-1}$. Fig. 9 shows the difference in averaged *SNR* between the $\Delta\beta$-drift model and HoP-drift model as a function of fiber crosstalk strength, when applying SVD and using 2 × 1 MISO to compensate for the residual modal coupling. We observe that the difference in *SNR* after equalization is large for lower crosstalk values, and then decreases as the fiber crosstalk strength increases towards the strong coupling regime (> -10 dB/km) as observed for the single-frequency case in Section IV.

VI. Conclusion

This paper develops a solution method for the coupled linear differential equations that describe the linear modal coupling in multi-mode fibers to account for environmentally induced slow channel drifting. The drift model is shown to be applicable to all linear coupling regimes, including to the intermediate regime that is most relevant to conventional few-mode fibers. The model proposed is shown to decorrelate the channel while keeping the mode coupling strength characteristic to all mode pairs, which is similar to the experimental observation in [28]. The dynamic channel model applicability is confirmed considering 16-QAM transmission and equalization using an SVD-based MISO system. We show the advantage that if intermodal coupling is compensated by SVD, then even in the presence of environmental drift just a 2 × 1 MISO equalizer is sufficient to compensate for the residual coupling reducing the complexity.

The drift model introduced here offers new insight into the modelling and development of future high-capacity SDM systems, in particular for few-mode and multi-mode fibers operating in the intermediate coupling regime. Critically, it supports the applicability of channel diagonalization schemes to increase spatial cardinality in SDM transmission systems at reduced MISO equalization complexity. In future, we will be looking towards verifying the presented model experimentally in our laboratory.

VII. Acknowledgment

The authors would like to acknowledge Dr. Zun Htay for the discussions and comments on the work. This work was supported by the UKRI Future Leaders Fellowship [MR/T041218/1]; Engineering and Physical Sciences Research Council (EPSRC) Doctoral Studentship Grant reference [EP/R513143/1] and [EP/W524335/1]. To access the underlying data for this publication, see: https://doi.org/10.5522/04/23868498.

References

[1] D. J. Richardson, J. M. Fini, and L. E. Nelson, "Space-division multiplexing in optical fibres," *Nature Photonics*, vol. 7, no. 5, pp. 354-362, 2013/05/01 2013, doi: 10.1038/nphoton.2013.94.

[2] B. J. Puttnam, G. Rademacher, and R. S. Luís, "Space-division multiplexing for optical fiber communications," *Optica*, vol. 8, no. 9, pp. 1186-

1203, 2021/09/20 2021, doi: 10.1364/OPTICA.427631.

[3] W. Klaus, P. J. Winzer, and K. Nakajima, "The Role of Parallelism in the Evolution of Optical Fiber Communication Systems," *Proceedings of the IEEE*, vol. 110, no. 11, pp. 1619-1654, 2022, doi: 10.1109/JPROC.2022.3207920.

[4] H. Srinivas, O. Krutko, and J. M. Kahn, "Efficient Integrated Multimode Amplifiers for Scalable Long-Haul SDM Transmission," *Journal of Lightwave Technology*, pp. 1-14, 2023, doi: 10.1109/JLT.2023.3254305.

[5] F. Ferreira, D. Fonseca, and H. J. A. Silva, "Design of few-mode fibers with M-modes and low differential mode delay," *Journal of Lightwave Technology*, vol. 32, no. 3, pp. 353--360, 2 2014, doi: 10.1109/JLT.2013.2293066.

[6] P. Sillard *et al.*, "55-Spatial-Mode Fiber for Space Division Multiplexing," in *2023 Optical Fiber Communications Conference and Exhibition (OFC)*, 5-9 March 2023 2023, pp. 1-3, doi: 10.1364/OFC.2023.M4B.5.

[7] G. Li, N. Bai, N. Zhao, and C. Xia, "Space-division multiplexing: the next frontier in optical communication," *Advances in Optics and Photonics*, vol. 6, no. 4, pp. 413-487, 2014/12/31 2014, doi: 10.1364/AOP.6.000413.

[8] F. M. Ferreira and F. A. Barbosa, "Maximizing the capacity of graded-index multimode fibers in the linear regime," *Journal of Lightwave Technology*, pp. 1-8, 2023, doi: 10.1109/JLT.2023.3324611.

[9] R. Maruyama, N. Kuwaki, S. Matsuo, and M. Ohashi, "Relationship Between Mode Coupling and Fiber Characteristics in Few-Mode Fibers Analyzed Using Impulse Response Measurements Technique," *Journal of Lightwave Technology*, vol. 35, no. 4, pp. 650-657, 2017, doi: 10.1109/JLT.2016.2609002.

[10] C. Antonelli, A. Mecozzi, and M. Shtaif, "The delay spread in fibers for SDM transmission: dependence on fiber parameters and perturbations," *Opt. Express*, vol. 23, no. 3, pp. 2196-202, 2015, doi: 10.1364/OE.23.002196.

[11] F. M. Ferreira, C. S. Costa, S. Sygletos, and A. D. Ellis, "Semi-Analytical Modelling of Linear Mode Coupling in Few-Mode Fibers," *J. Light. Technol.*, vol. 35, no. 18, pp. 4011-4022, 2017, doi: 10.1109/jlt.2017.2727441.

[12] M. Fridman, H. Suchowski, M. Nixon, A. A. Friesem, and N. Davidson, "Modal dynamics in multimode fibers," *J. Opt. Soc. Am. A*, vol. 29, no. 4, pp. 541-544, 2012/04/01 2012, doi: 10.1364/JOSAA.29.000541.

[13] C. B. Czegledi, M. Karlsson, E. Agrell, and P. Johannisson, "Polarization drift channel model for coherent fibre-optic systems," *Scientific reports*, vol. 6, no. 1, p. 21217, 2016.

[14] F. A. Barbosa and F. M. Ferreira, "On the advantages of principal modes for multimode SDM transmission systems," in *Optical Fiber Communication Conference*, 2023: Optica Publishing Group, p. Th2A. 31.

[15] G. Rademacher *et al.*, "Channel Dynamics in Few-Mode Fiber Transmission Under Mechanical Vibrations," in *Optical Fiber Communication Conference (OFC) 2020*, San Diego, California, 2020/03/08 2020: Optica Publishing Group, in OSA Technical Digest, p. Th1H.3, doi: 10.1364/OFC.2020.Th1H.3.

[16] X. Chen, J. He, A. Li, J. Ye, and W. Shieh, "Characterization and Analysis of Few-Mode Fiber Channel Dynamics," *IEEE Photonics Technology Letters*, vol. 25, no. 18, pp. 1819-1822, 2013, doi: 10.1109/LPT.2013.2275249.

[17] P. M. Krummrich, E.-D. Schmidt, W. Weiershausen, and A. Mattheus, "Field Trial Results on Statistics of Fast Polarization Changes in Long Haul WDM Transmission Systems," in *Optical Fiber Communication Conference and Exposition and The National Fiber Optic Engineers Conference*, Anaheim, California, 2005/03/06 2005: Optical Society of America, in Technical Digest (CD), p. OThT6.

[18] G. M. Saridis *et al.*, "Dynamic skew measurements in 7, 19 and 22-core multi core fibers," in *2016 21st OptoElectronics and Communications Conference (OECC) held jointly with 2016 International Conference on Photonics in Switching (PS)*, 3-7 July 2016 2016, pp. 1-3.

[19] G. Rademacher, R. S. Luís, B. J. Puttnam, Y. Awaji, and N. Wada, "Crosstalk dynamics in multi-core fibers," *Optics Express*, vol. 25, no. 10, pp. 12020-12028, 2017/05/15 2017, doi: 10.1364/OE.25.012020.

[20] P. M. Krummrich, C. Spenner, and K. Petermann, "Dynamic linear mode coupling effects in multi mode fibers for mode division multiplexed transmission (invited)," in *2022 IEEE Photonics Society Summer Topicals Meeting Series (SUM)*, 11-13 July 2022 2022, pp. 1-2, doi: 10.1109/SUM53465.2022.9858227.

[21] K. Choutagunta and J. M. Kahn, "Dynamic Channel Modeling for Mode-Division Multiplexing," *Journal of Lightwave Technology*, vol. 35, no. 12, pp. 2451-2463, 2017, doi: 10.1109/JLT.2017.2656821.

[22] F. A. Barbosa and F. M. Ferreira, "Scaling Spatial Multiplexing with Principal Modes," in *2022 IEEE Photonics Conference (IPC)*, 2022: IEEE, pp. 1-2.

[23] A. Mecozzi *et al.*, "Use of Optical Coherent Detection for Environmental Sensing," *Journal of Lightwave Technology*, vol. 41, no. 11, pp. 3350-3357, 2023/06/01 2023.

[24] P. Boffi *et al.*, "Mode-Group Division Multiplexing: Transmission, Node Architecture, and Provisioning," *Journal of Lightwave Technology*, vol. 40, no. 8, pp. 2378-2389, 2022, doi: 10.1109/JLT.2021.3135636.

[25] A. Vijay and J. M. Kahn, "Effect of Higher-Order Modal Dispersion in Direct-Detection Mode-Division-Multiplexed Links," *Journal of Lightwave Technology*, vol. 41, no. 6, pp. 1670-1683, 2023, doi: 10.1109/JLT.2022.3226704.

[26] K. Choutagunta, I. Roberts, and J. M. Kahn, "Efficient Quantification and Simulation of Modal Dynamics in Multimode Fiber Links," *Journal of Lightwave Technology*, vol. 37, no. 8, pp. 1813-1825, 2019, doi: 10.1109/JLT.2018.2889675.

[27] F. M. Ferreira, C. S. Costa, S. Sygletos, and A. D. Ellis, "Nonlinear performance of few-mode fiber links with intermediate coupling," *Journal of Lightwave Technology*, vol. 37, no. 3, pp. 989-999, 2019.

[28] J. Carpenter, B. J. Eggleton, and J. Schröder, "Observation of Eisenbud–Wigner–Smith states as principal modes in multimode fibre," *Nature Photonics*, vol. 9, no. 11, pp. 751-757, 2015.

[29] F. A. Barbosa and F. M. Ferreira, "On a Scalable Path for Multimode SDM Transmission," *Journal of Lightwave Technology*, pp. 1-10, 2023, doi: 10.1109/JLT.2023.3308777.

[30] R. Yadav, F. A. Barbosa, and F. M. Ferreira, "Dynamic Channel Modelling for Multimode Fibre Links in All Linear Coupling Regimes " in *European Conference on Optical Communications*, Glassgow, 2023: IEEE, pp. 1-3.

[31] D. Marcuse, *Theory of Dielectric Optical Waveguides*. Academic Press, 1991.

[32] M. B. Shemirani, W. Mao, R. A. Panicker, and J. M. Kahn, "Principal Modes in Graded-Index Multimode Fiber in Presence of Spatial- and Polarization-Mode Coupling," *Journal of Lightwave Technology*, vol. 27, no. 10, pp. 1248-1261, 2009, doi: 10.1109/jlt.2008.2005066.

[33] K.-P. Ho and J. M. Kahn, "Mode Coupling and its Impact on Spatially Multiplexed Systems," pp. 491-568, 2013, doi: 10.1016/b978-0-12-396960-6.00011-0.

[34] C. Antonelli, G. Riccardi, T. Hayashi, and A. Mecozzi, "Role of polarization-mode coupling in the crosstalk between cores of weakly-coupled multi-core fibers," *Optics Express*, vol. 28, no. 9, pp. 12847-12861, 2020/04/27 2020, doi: 10.1364/OE.391092.

[35] H. Kogelnik and P. J. Winzer, "Modal birefringence in weakly guiding fibers," *Journal of Lightwave Technology*, vol. 30, no. 14, pp. 2240-2245, 2012, doi: 10.1109/JLT.2012.2193872.

[36] W. Xiong, C. W. Hsu, Y. Bromberg, J. E. Antonio-Lopez, R. Amezcua Correa, and H. Cao, "Complete polarization control in multimode fibers with polarization and mode coupling," *Light: Science & Applications*, vol. 7, no. 1, p. 54, 2018/08/08 2018, doi: 10.1038/s41377-018-0047-4.

[37] K.-P. Ho and J. M. Kahn, "Linear Propagation Effects in Mode-Division Multiplexing Systems," *J. Light. Technol.*, vol. 32, no. 4, pp. 614-628, 2014, doi: 10.1109/jlt.2013.2283797.

[38] L. Dallachiesa *et al.*, "Mode-Group-Division Multiplexing over a Deployed 15-Mode-Fiber Cable," in *Optical Fiber Communication Conference (OFC) 2023*, San Diego California, 2023/03/05 2023: Optica Publishing Group, in Technical Digest Series, p. M2B.4, doi: 10.1364/OFC.2023.M2B.4

[39] J. Carpenter, B. C. Thomsen, and T. D. Wilkinson, "Degenerate mode-group division multiplexing," *Journal of Lightwave Technology*, vol. 30, no. 24, pp. 3946-3952, 2012.

[40] L. Gruner-Nielsen *et al.*, "Few Mode Transmission Fiber With Low DGD, Low Mode Coupling, and Low Loss," *J. Light. Technol.*, vol. 30, no. 23, pp. 3693-3698, 2012, doi: 10.1109/jlt.2012.2227243.

[41] T. Mori, T. Sakamoto, M. Wada, T. Yamamoto, and F. Yamamoto, "Low DMD four LP mode transmission fiber for wide-band WDM-MIMO system," in *Proc. OFC*, 2013, p. OTh3K.1, doi: 10.1364/OFC.2013.OTh3K.1.

[42] N. K. Fontaine, R. Ryf, M. Hirano, and T. Sasaki, "Experimental investigation of crosstalk accumulation in a ring-core fiber," in *2013 IEEE Photonics Society Summer Topical Meeting Series*, 8-10 July 2013 2013, pp. 111-112, doi: 10.1109/PHOSST.2013.6614511.

[43] R. Ryf *et al.*, "Space-Division Multiplexed Transmission over 4200 km 3-Core Microstructured Fiber," in *Proc. OFC*, 2012, p. PDP5C.2, doi: 10.1364/NFOEC.2012.PDP5C.2.

[44] L. Mazzoleni, A. G. Demir, L. Caprio, M. Pacher, and B. Previtali, "Real-time observation of melt pool in selective laser melting: Spatial, temporal, and wavelength resolution criteria," *IEEE Transactions on Instrumentation and Measurement*, vol. 69, no. 4, pp. 1179-1190, 2019.

[45] C. D. Poole and J. Nagel, "Chapter 6 - Polarization Effects in Lightwave Systems," in *Optical Fiber Telecommunications IIIA (Third Edition)*, I. P. Kaminow and T. L. Koch Eds. Boston: Academic Press, 1997, pp. 114-161.

[46] T. Xu *et al.*, "Frequency-Domain Chromatic Dispersion Equalization Using Overlap-Add Methods in Coherent Optical System," vol. 32, no. 2, pp. 131-135, 2011, doi: doi:10.1515/joc.2011.022.

[47] P. Parolari *et al.*, "Demonstration of Multi-Hop Mode-Group Routing in a Field-Deployed Multi-Mode Fiber Network," in *2023 Optical Fiber Communications Conference and Exhibition (OFC)*, 2023: IEEE, pp. 1-3.

[48] R. Ryf *et al.*, "23 Tbit/s transmission over 17-km conventional 50-μm graded-index multimode fiber," in *Optical Fiber Communication Conference*, 2014: Optica Publishing Group, p. Th5B. 1.